

Development of An Electrochemical Impedance Immunosensor for Myoglobin Determination

Libo Sun¹, Wenwen Li², Maojing Wang³, Wei Ding⁴ and Yang Ji^{3,*}

¹ Department of Pharmacy, The Affiliated Hospital of Qingdao University, Qingdao, Shandong, P.R. China

² Department of Hematology, Qingdao Commercial staff Hospital, Qingdao, Shandong, P.R. China

³ Department of Cardiology, The Affiliated Hospital of Qingdao University, Qingdao, Shandong, P.R. China

⁴ Ophthalmology Department, Huangdao District People's Hospital, P.R. China

*E-mail: yangji_168@foxmail.com

Received: 28 March 2017 / Accepted: 6 May 2017 / Published: 12 June 2017

This work addressed the fabrication of a bioelectrode via the attachment of monolayer-protected Au nanoparticles (AuNPs) onto a 3-aminopropyltriethoxysilane (APTES) self-assembled monolayer (SAM) on an indium-tin-oxide (ITO). An anti-myoglobin antibody (Ab-Mb) was then linked to the AuNPs with a carbodiimide coupling reaction. The terminal bioelectrode was termed as Ab-Mb/AuNPs/APTES/ITO. Electrochemical impedance spectroscopy (EIS) and cyclic voltammetry (CV) were employed for the characterization of the proposed bioelectrode, which displayed an electrochemical impedance response to Ag-Mb in phosphate buffer solution (PBS) with a linear range of 10 ng/mL-1 µg/mL and an LOD of 2.7 ng/mL.

Keywords: Myoglobin; Gold nanoparticles; Impedance immunosensor; Electrochemical impedance spectroscopy; Bioelectrode

1. INTRODUCTION

Cardiac myoglobin (Mb) is among the earliest biomolecules released into blood circulation after acute myocardial infarction (AMI) and is, therefore, an early marker for AMI. The level of an early marker within 6 h after symptoms onset and a definitive marker with remarkable sensitivity and specificity in blood could be employed for AMI diagnostics, as recommended by the National Academy of Clinical Biochemistry (NACB) [1, 2]. Myoglobin is rapidly released, circulated and shows an increase in concentration due to its small size (17.8 kDa). It is unusual for the serum

concentration of myoglobin to exceed 110 $\mu\text{g/L}$, and this is an indication for AMI. Although performing well in sensitivity with an LOD of no less than 1 $\text{ng}\cdot\text{mL}^{-1}$, ELISA and other cardiac markers detection assays are considered improper for rapid decision-making with respect to heart attack, since these assays require no less than 6 h to conduct, and they must be performed in central laboratories of hospitals and clinics. In addition, a large number of reagents and specimens are required in these large-scale assays. Early, on-site diagnostics with desirable accuracy aid doctors in their diagnoses. Novel techniques need to be developed for fast biomarker determinations. In terms of on-site diagnostics, electrochemical biosensors/immunosensors are a present area of interest. Featuring cost-effectiveness, facile miniaturization and desirable specificity, and sensitivity and simplicity, electrochemical immunosensors have gained widespread recognition as a promising analysis technique.

Being portable, highly efficient, easily usable, possible to be miniaturized, rapid in response time, and direct in transduction (biomolecular recognition events directly leading to electronic signals), electrochemical immunosensors have triggered a revolution in contemporary chemical analysis as a significant sensing system. Electrochemical immunosensors have gained extensive use in biological-warfare agents, biological toxins, biomarker and protein detection in the fields of pharmaceutical chemistry, environment, food and clinical diagnosis applications since they are significantly cost-effective, selective, sensitive and accurate [3-7]. On the basis of glassy carbon electrode (GCE) modified by methylene blue-multiwalled carbon nanotubes (MWCNT) nanohybrid, an Mb-targeted electrochemical sensor was proposed by Pakapongpan and co-workers [8], with direct electrochemical reduction of Mb as the basis of determination. The linear range of Mb determination was as extensive as 0.1 μM -3.0 μM ($\sim 1.78 \mu\text{g mL}^{-1}$ -53.40 $\mu\text{g mL}^{-1}$) with respect to the proposed biosensor. It is, however, still beyond the physiological range of cMb in human blood. Hence, the specimen should be diluted when applied to sub- $\mu\text{g mL}^{-1}$ Mb determination. Since the sensing formation of antibody-antigen and biotin-avidin complexes and DNA-oligonucleotide interactions and other biological interfaces have witnessed the nondestructive and sensitive performance of electrochemical impedance spectroscopy (EIS) in characterizing electrical traits, much attention has been paid to this technique [9, 10].

Having gained widespread application in the field of electrochemical sensors, Au nanoparticles could take the roles of either markers in electrochemical determination or a desirable conducting medium for electron exchange rate facilitation [11]. Au nanomaterials of varying forms have been presented in various publications to immobilize redox proteins, where direct electrochemistry has been achieved. The direct electrochemistry of hemoglobin (Hb) was studied on an Au nanowire array by Yang and co-workers [12]. To study the electrochemical performance of Hb, polyvinyl alcohol and 1-octyl-3-methylimidazolium hexafluorophosphate were integrated with an Au nanoparticle by Zhang and co-workers [13]. With Hb immobilized onto a single-dimensional Au nanoparticle, a new amperometric biosensor was fabricated by Hong and co-workers [14]. Au nanoparticles have also been applied in the field of electrochemical DNA biosensors. The activity concerning immobilized biomolecules, electrocatalytic activity-induced electron exchange rate promotion, as well as the enhancement in DNA hybridization and immobilization ability could be realized by the existence of Au nanoparticles on the surface of an electrode [15, 16].

To fabricate a bioelectrode to determine Mb as a cardiac biomarker, a platform with functionalized Au nanoparticles was employed in this study, with full consideration of the strengths of metal Au nanoparticle traits as well as an EIS strategy. The covalent anchoring of the nanoparticles occurs on the self-assembled monolayer (SAM) of 3-aminopropyltriethoxy silane (APTES) over an indium-tin-oxide (ITO) glass plate. Using carbodiimide coupling, Ab-cMb (cardiac protein antibody) was covalently attached to APTES/ITO glass plates decorated with carboxyl-functionalized Au nanoparticles. Diverse microscopic strategies were employed for systematic characterization of the proposed bioelectrode. EIS with the redox probe $[\text{Fe}(\text{CN})_6]^{3-/4-}$ was employed for the investigation of the capacity of this bioelectrode to quantitatively estimating Ag-Mb in phosphate buffered saline (PBS) at pH 7.4.

2. EXPERIMENTS

2.1. Chemicals

Sigma-Aldrich Corp was the source for monoclonal mouse anti-human cardiac myoglobin (Ab-Mb), 3-mercaptopropionic acid (MPA), sodium borohydride (NaBH_4), chloroauric acid (HAuCl_4), *N*-hydroxysuccinimide 98% (NHS), 3-mercaptopropyltrimethoxysilane (MPMSi), *N*-(3-dimethyl aminopropyl)-*N'*-ethylcarbodiimide hydrochloride (EDC), 3-aminopropyltriethoxysilane (APTES), mouse immunoglobulin-G (Ag-IgG) and human heart tissue-derived myoglobin (Ag-Mb). Myoglobin standards and the human myoglobin ELISA kit were purchased from Abcam (Shanghai, China). The remaining reagents were of analytical grade and were employed with no additional purification.

2.2. Synthesis of monolayer-protected gold nanoparticles

Monolayer-protected Au nanoparticles were prepared and purified through the Weller reaction [17], with MPMSi in a thiol/ AuCl_4^- mole ratio of 1:1 in 2-propanol. This was followed by the addition of NaBH_4 as a reducing agent cooled to 273 K using an ice water bath for 1 h. The terminal monolayer-protected Au nanoparticle solution was filtered through PTFE membranes (0.2 μm) for deposition removal, and then the excess 2-propanol was evaporated in a rotary evaporator. This was followed by the separation and collection of the crude product of Au nanoparticles via centrifugation. The Au nanoparticles were then washed with ethanol to remove the unreacted thiols and byproducts.

2.3. Preparation of immunosensor

The ITO-coated glass was ultrasonically cleaned successively in Extran, acetone, ethanol, isopropyl alcohol and DI water, with vacuum drying following each cleaning process. To raise the number of hydroxyl groups on the surface of the ITO glass, the cleaned plates were subsequently exposed to oxygen plasma in a plasma chamber for 5 min. This was followed by immersion of the glass plates into a 2% ethanolic APTES solution for 90 min at room temperature to obtain APTES-

SAM. After rinsing with ethanol, non-bonded APTES was removed from the substrate surface together with N₂ gas flow drying. Aqueous AuNPs (5 mL, 0.1 mg/mL) was added with NHS (30 mM) and EDC (150 mM) to activate carboxyl groups. The ITO glass plates were immersed into the mixture of functionalized and activated AuNPs for 60 min, washed with doubly distilled water, and dried under N₂ gas flow to give AuNPs/APTES/ITO. The electrode was treated overnight with PBS (pH 7.4) containing Ab-Mb (100 µg/mL) at 4 °C. This was followed by PBS washing and N₂ flow drying. Subsequently, the incubation of the Ab-Mb-immobilized electrode was performed in a BSA solution (1%) for 0.5 h to block the nonspecific binding sites on the surface of the electrode, followed by PBS washing to remove any physically adsorbed antibodies. The final immunosensor, denoted as Ab-Mb/AuNPs/APTES/ITO, was dried with N₂.

2.4. Characterization and measurement

An SM-240 CCD spectrophotometer (CVI Spectral Instruments, Putnam, CT, USA) was used to characterize Au and blank nanoparticles in solution via UV–vis absorption spectra. A traditional triple-electrode system was applied to the electrochemical measurements, where the roles of counter, reference and working electrode were taken by platinum wire, Ag/AgCl and the prepared electrode. Cyclic voltammetry was conducted in 10.0 mL of 0.1 M KCl containing 1.0 mM each of Fe(CN)₆³⁻ and Fe(CN)₆⁴⁻ at a scan rate of 50 mV/s. Electrochemical impedance spectroscopy (EIS) measurements with a frequency range of 1-100 kHz at an AC voltage of 0.05 V were performed in PBS, pH 7.4, containing 0.1 M KCl and 2 mM [Fe(CN)₆]³⁻/[Fe(CN)₆]⁴⁻.

3. RESULTS AND DISCUSSION

Figure 1 shows the UV absorption spectra of Au nanoparticles protected by the monolayer. Both the ~525 nm absorption band and yellow-brownish red color variation in the mixture of MPMSi + AuCl₄⁻ solution provide convincing evidence for successful Au nanoparticles synthesis. Since the mercapto group of MPMSi has significant affinity to Au, a rather narrowed size is attained for the tiny Au nanoparticles [18]. Based on the SPR location, the size of the Au NPs can be estimated to be 14 nm. Thus, Au nanoparticles are ensured in this way, with the following aminofunctionalization of them facilitated. Moreover, the elevated ratio of surface-to-volume and nonrandom nanostructure has been displayed for the Au nanoparticles according to the aforementioned results. Hence, protein immobilization could be achieved via the two traits of the nanoparticles for subsequent electrochemical sensor preparation.

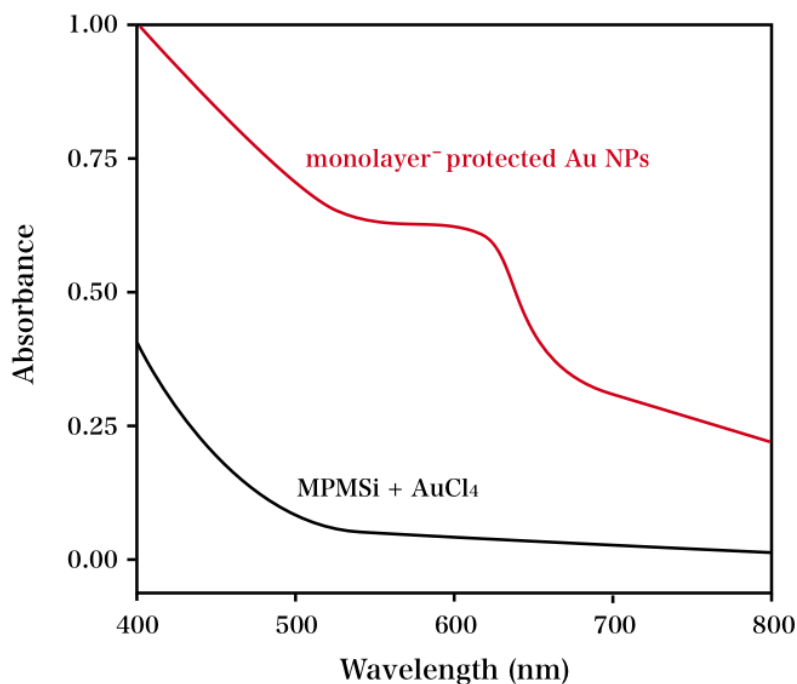


Figure 1. UV/vis spectra of the colloidal solution of Au nanoparticles in 2-propanol and the unreacted 2-propanol solution with MPMSi and AuCl₄⁻ (S/Au ratio of 1:1).

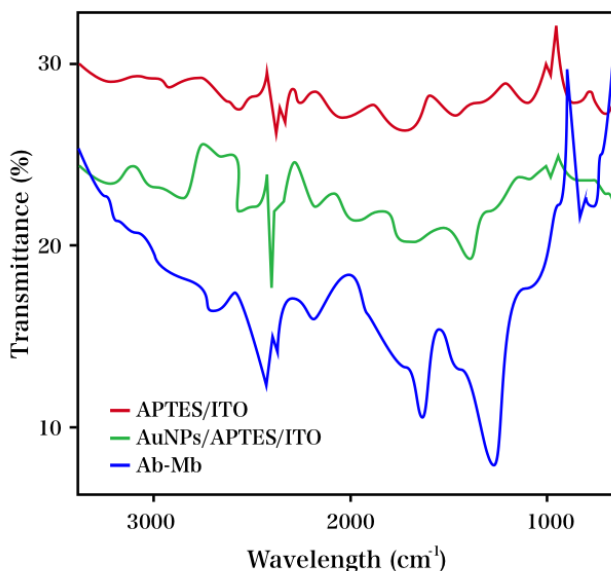


Figure 2. FTIR spectra of APTES/ITO, AuNPs/APTES/ITO and Ab-Mb/AuNPs/APTES/ITO.

Under attenuated total reflection mode, FTIR measurement is employed to characterize Ab-Mb/AuNPs/APTES/ITO, AuNPs/APTES/ITO and APTES/ITO. Their respective spectra are shown in

Figure 2. A Si–O–Si characteristic band is observed at 1055 cm^{-1} in for APTES. C=O stretching vibrations of the carboxylic groups of AuNPs account for the band at 1748 cm^{-1} . The –OH bending and stretching vibrations of carboxylic acid groups are respectively reflected by the 939 and 2962 cm^{-1} peaks. The N–Au vibration mode has been noticed at 1044 cm^{-1} , suggesting the affliction of the nitrogen and gold bonding during the synthesis process. The N–H bending and stretching vibrations are seen in the peaks observable at 1612 and 3387 cm^{-1} , showing successful Ab-Mb immobilization [19].

We examined the properties of the decorated electrode surface facily and effectively via cyclic voltammetry measurement. Electron transfer resistance and other electron exchange rate constants bear theoretical relation with the variations in peak current and separation of peak potentials on varying electrode surfaces, as reflected in cyclic voltammograms (CVs). With the redox probe consisting of a $[\text{Fe}(\text{CN})_6]^{3-/4-}$ mixture in PBS (containing 0.1 M KCl), pH of 7.4 , cyclic voltammetry was employed for the surveillance of every stage of antibody immobilization as well as ITO surface modification. CV profiles preceding and succeeding each step of electrode surface modification are shown in Figure 3. Ab-Mb/AuNPs/APTES/ITO is formed due to the subsequent Ab-Mb immobilization. The original ITO exhibits a peak-to-peak separation between the oxidation and reduction potentials (ΔE_p) of 125 mV via a quasi-reversible CV. This is followed by a decline to 96 mV (ΔE_p) after APTES-SAM-induced modification. These changes are attributed to an increased interfacial concentration of the anionic probe ($[\text{Fe}(\text{CN})_6]^{3-/4-}$) due to its strong affinity toward the polycationic (NH_3^+) layer of the amino groups of the APTES [20]. Nevertheless, with respect to AuNPs-decorated APTES/ITO, there is a rise in peak potential and, conversely, a decline in peak current. Both after blocking with BSA and with Ab-Mb immobilization on the AuNPs/APTES/ITO surface, there is an additional decline in CV peak current, possibly ascribed to the generation of a protein-antibody layer on the electrode. Herein, the route for redox probe to electrode surface is remarkably impeded by this layer that obstructs mass-transfer and electron exchange.

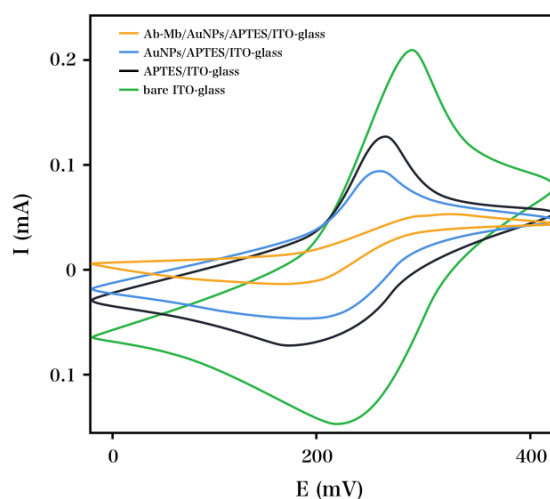


Figure 3. CV of the original ITO; APTES/ITO; AuNPs/APTES/ITO; Ab-Mb/ZnS(MPA)/APTES/ITO glass as well as Ab-Mb/AuNPs/APTES/ITO in PBS, pH 7.4 , containing $2\text{ mM } [\text{Fe}(\text{CN})_6]^{3-/4-}$ plus 0.1 M KCl .

Because the electrochemical courses at the solution/electrode interface concerning the decorated electrodes can be quantitatively and qualitatively characterized by EIS measurements, it was selected as the major characterization approach to evaluate immunosensor behavior. We detected its response to AC signal (small amplitude) adoption at varying frequencies via EIS. The impedance performance of varying decorated electrodes is indicated in Nyquist plots with Z' (real part of the impedance) vs. $-Z''$ (imaginary part of the impedance). In contrast, the linear portion coinciding with the diffusion limited electron shift occurred at comparatively lower frequencies. It can be proposed that the spectra were similar to those of Randle's equivalent circuit in theory. Diverse decorated electrodes are characterized via Nyquist plots with equivalent circuits (inset Figure 4). The R_{et} value with respect to the original ITO is observed at $84.12 \Omega \text{ cm}^2$, while that with respect to APTES/ITO greatly declines to $22.59 \Omega \text{ cm}^2$. Since the anionic probe $[\text{Fe}(\text{CN})_6]^{3-/4-}$ has significantly affinity for the polycationic layer, as the amino groups of APTES are protonated (NH_3^+) in aqueous solution, there is an increase in the concentration of the probe, thus reducing the R_{et} value. Since the negatively-charged AuNPs carboxyl species at the interface of the solution and electrode are charge repulsive, there is a significant increase in the R_{et} value up to $110.4 \Omega \text{ cm}^2$ after AuNPs are attached to the silane layer. The probe-electrode surface electron exchange is unrestricted, as suggested by the finding that an obvious R_{et} decline down to $17.0 \Omega \text{ cm}^2$ corresponds to the decline in semicircle diameter with respect to AuNPs/APTES/ITO. Moreover, the distinct R_{et} increase to $199.3 \Omega \text{ cm}^2$ is attributed to MB antibody immobilization onto AuNPs over the surface of the electrode as well as the obstruction of the BSA-induced nonspecific binding sites. The probe-electrode surface mass and charge exchange is impeded due to the insulation property of the protein molecule.

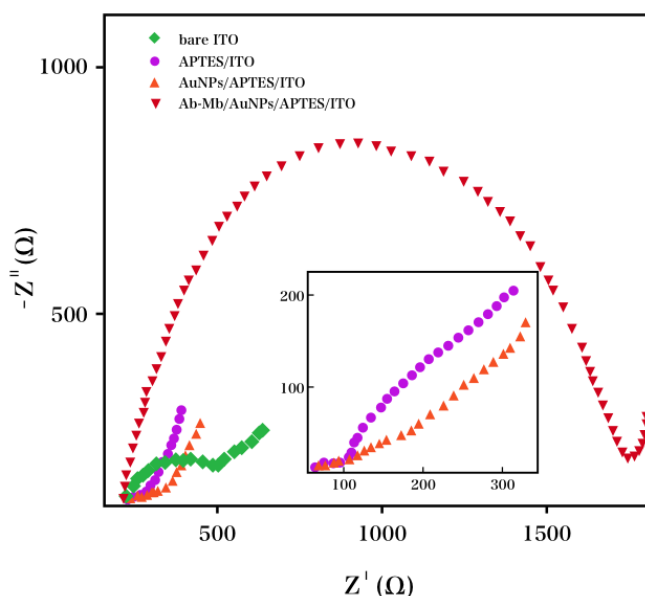


Figure 4. Nyquist plots of original ITO; APTES/ITO; AuNPs/APTES/ITO as well as Ab-Mb/AuNPs/APTES/ITO in PBS (pH 7.4) containing 2 mM $[\text{Fe}(\text{CN})_6]^{3-/4-}$ plus 0.1 M KCl.

Non-Faradaic impedance biosensors perform impedance measurement in the absence of any redox probe. Bacteria detection is based on the impedance change upon the attachment of bacterial cells on an interdigitated microelectrode in the absence of any redox probe in the sample solution. An antigen-antibody complex is formed by the specific immunoreaction between Ab-Mb and Ag-Mb, where the latter functions as the complementary target of the former. The interfacial electron exchange at the interface of the solution and bioelectrode is interrupted by an immunocomplex-induced kinetic barrier. There is an increase in electron exchange resistance, together with a decrease in capacitance, with gradually impeded Faradaic reaction of the redox couple. The control group uses an Ag-Mb-free sample solution, with an R_{et} value recorded as the control sample response. After aliquots of target protein antigen with varying concentrations are consecutively added, the corresponding Nyquist plots obtained are shown in Figure 5A. As the added Ag-Mb increases in concentration, Nyquist circles exhibit a significant increase in diameter.

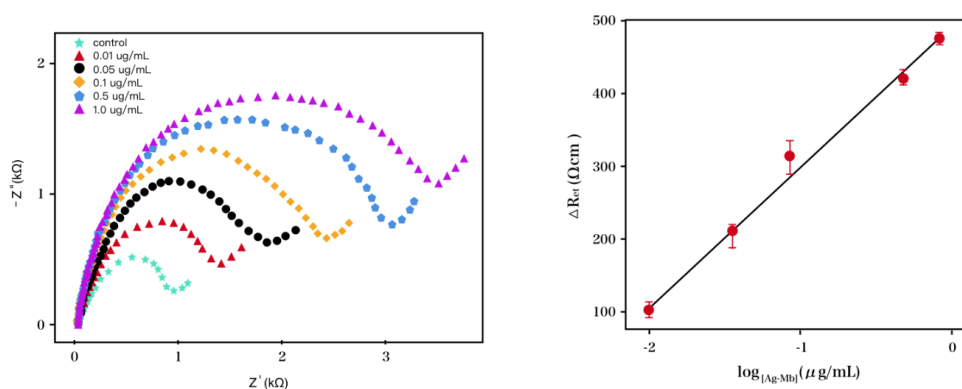


Figure 5. (A) Faradaic impedance spectra of the Ab-Mb/AuNPs/APTES/ITO preceding and succeeding incubation with varying concentrations of Ag-Mb in PBS, pH 7.4, containing 2 mM $[\text{Fe}(\text{CN})_6]^{3-/4-}$ plus 0.1 M KCl. (B) Concentration dependent calibration profile with respect to the bioelectrode.

Table 1. Performance comparison of the Ab-Mb/AuNPs/APTES/ITO and other Mb electrochemical sensor.

Method	Linear range	Detection limit	Reference
Bio-functionalized Pt NPs	0.01 μg/mL-1 μg/mL	4 ng/mL	[23]
TiO ₂ nanotubes	—	50 nM	[24]
Au/graphene/carbon ionic liquid electrode	1.98-238.2 μM	0.66 μM	[25]
Fe ₃ O ₄ @SiO ₂ microsphere/carbon ionic liquid electrode	0.2-11 mM	0.18 mM	[26]
Ab-Mb/AuNPs/APTES/ITO	10 ng/mL-1 μg/mL	2.7 ng/mL	This work

This is ascribed to the interaction between antibody and antigen. The variation in specific electron charge exchange resistance *versus* the logarithmic Ag-Mb concentration (10 ng/mL-1 μg/mL) is plotted for the bioelectrode in Figure 5B, with an LOD of 2.7 ng/mL based on a signal-to-noise ratio

of 3:1. EIS has the potential to be employed for clinical determination due to its comparatively short experimental course time (roughly 15 min) for the entire assay, in comparison with ELISA, which requires several days. Hence, among other recently issued polymer-based Mb sensors as well as semiconductor/metal nanoparticle/carbon nanomaterials, the proposed bioelectrode is the most desirable platform [8, 21, 22]. The sensing performance of the new sensor was compared with recently reported sensors, as shown in Table 1.

Mb was determined in spiked, diluted (1:10) synthetic serum samples and EIS measurements were performed. The linear detection range is from 50 ng/mL to 700 ng/mL. In all measurements, the repeatability is always less than 6%. Each target Ag-Mb with varying concentration was added for ten diverse independently fabricated bioelectrodes. This work thus successfully assessed bioelectrode reproducibility. Desirable preparation reproducibility as well as precision are displayed by the inter-assay variation coefficient range of 2–12% at an individual Ag-Mb concentration. The impedance measurements were repeatedly performed for target Ag-Mb with the same concentration on the bioelectrode in similar conditions to examine stability. The embodiment of bioelectrode biocompatibility in either open air or solution is indicated by the absence of observable impedimetric response variations, even after 5 impedance measurements were conducted. The immunoreactions in the presence of nonspecific mouse IgG under similar conditions were performed to examine the specificity of the bioelectrode for Ag-Mb, without obvious R_{et} variations monitored as aliquots of IgG was added, possibly due to the attenuated nonspecific interaction or the absence of the interaction between antibody and antigen, thus verifying the specificity of the proposed bioelectrode.

Table 2. The contents and recoveries of Mb detected in synthetic serum samples (n=3).

Sample	Added (ng/mL)	Found (ng/mL)	ELISA result (nM/mL)	Recovery (%)	RSD (%)
1	70	68.7	69.1	98.14	3.6
2	150	154.6	147.2	98.13	2.5
3	300	309.9	295.7	103.3	1.9

4. CONCLUSIONS

Here, we have given an integrated study of an AuNPs-based bioelectrode employed in bioanalytical immunosensor application. In general, the monolayer-protected AuNPs were covalently attached over APTES-SAM onto the ITO surface. The electrode is not only desirably biocompatible but also supplies ample binding sites where Ab-Mb is immobilized on the surface of the electrode for immunoreaction. The detection range for Ag-Mb with respect to the prepared sensor is 10 $\mu\text{g/mL}$ in PBS.

References

1. A. Wu, F. Apple, W. Gibler, R. Jesse, M. Warshaw and R. Valdes, *Clinical Chemistry*, 45 (1999)

1104.

2. F. Apple, R. Jesse, L. Newby, A. Wu and R. Christenson, *Circulation*, 115 (2007) e352.
3. L. Bonel, J. Vidal, P. Duato and J. Castillo, *Biosensors and Bioelectronics*, 26 (2011) 3254.
4. B. Jeong, R. Akter, O. Han, C. Rhee and M. Rahman, *Anal. Chem.*, 85 (2013) 1784.
5. J. Li, L. Xiao, G. Zeng, G. Huang, G. Shen and R. Yu, *Journal of Agricultural and Food Chemistry*, 53 (2005) 1348.
6. S. Arya, T. Pui, C. Wong, S. Kumar and A. Rahman, *Langmuir*, 29 (2013) 6770.
7. Q. Wei, Y. Zhao, B. Du, D. Wu, H. Li and M. Yang, *Food Chemistry*, 134 (2012) 1601.
8. S. Pakapongpan, R. Palangsantikul and W. Surareungchai, *Electrochimica Acta*, 56 (2011) 6831.
9. A. Venkatanarayanan, T. Keyes and R. Forster, *Anal. Chem.*, 85 (2013) 2216.
10. S. Shrikrishnan, K. Sankaran and V. Lakshminarayanan, *J Phys Chem C*, 116 (2012) 16030.
11. C. Lei, S. Hu, G. Shen and R. Yu, *Talanta*, 59 (2003) 981.
12. M. Yang, F. Qu, Y. Li, Y. He, G. Shen and R. Yu, *Biosensors and Bioelectronics*, 23 (2007) 414.
13. Y. Zhang, R. Yan, F. Zhao and B. Zeng, *Colloids and Surfaces B: Biointerfaces*, 71 (2009) 288.
14. J. Hong and Z. Dai, *Sensors and Actuators B: Chemical*, 140 (2009) 222.
15. H. Gao, X. Qi, Y. Chen and W. Sun, *Anal. Chim. Acta.*, 704 (2011) 133.
16. J. Pingarrón, P. Yáñez-Sedeño and A. González-Cortés, *Electrochimica Acta*, 53 (2008) 5848.
17. A. Schroedter and H. Weller, *Angewandte Chemie International Edition*, 41 (2002) 3218.
18. T. Teranishi, I. Kiyokawa and M. Miyake, *Adv. Mater.*, 10 (1998) 596.
19. A. Barth, *Biochimica et Biophysica Acta (BBA)-Bioenergetics*, 1767 (2007) 1073.
20. J. Zhao, C.R. Bradbury, S. Huclova, I. Potapova, M. Carrara and D. Fermín, *J Phys Chem B*, 109 (2005) 22985.
21. E. Matveeva, Z. Gryczynski and J. Lakowicz, *Journal of immunological methods*, 302 (2005) 26.
22. E. Suprun, A. Shilovskaya, A. Lisitsa, T. Bulko, V.V. Shumyantseva and A.I. Archakov, *Electroanalysis*, 23 (2011) 1051.
23. S. Mishra, A. Srivastava and D. Kumar, *RSC Advances*, 4 (2014) 21267.
24. S. Mandal, K. Narayan and A. Bhattacharyya, *Journal of Materials Chemistry B*, 1 (2013) 3051.
25. G. Li, T. Li, Y. Deng, Y. Cheng, F. Shi, W. Sun and Z. Sun, *Journal of Solid State Electrochemistry*, 17 (2013) 2333.
26. X. Wang, Z. You, H. Sha, Z. Sun and W. Sun, *Journal of Solid State Electrochemistry*, 18 (2014) 207.